Pressure-induced large enhancement of Néel temperature and electric polarization in the hexagonal multiferroic Lu$_{0.5}$Sc$_{0.5}$FeO$_3$

Fengliang Liu,[1,2] Changsong Xu,[3] Shoudong Shen,[1] Nana Li,[2] Hangwen Guo,[4,5] Xujie Lü,[2] Hongjun Xiang,[1,5] L. Bellaiche,[3] Jun Zhao,[1] Lifeng Yin,[1,4,5] Wenge Yang,[2,*] Wenbin Wang,[4,5,†] and Jian Shen [1,4,5,‡]

[1]*State Key Laboratory of Surface Physics and Department of Physics, Fudan University, Shanghai 200433, China*
[2]*Center for High Pressure Science and Technology Advanced Research (HPSTAR), Shanghai 201203, China*
[3]*Physics Department and Institute for Nanoscience and Engineering, University of Arkansas, Fayetteville, Arkansas 72701, USA*
[4]*Institute for Nanoelectronic Devices and Quantum Computing, Fudan University, Shanghai 200433, China*
[5]*Collaborative Innovation Center of Advanced Microstructures, Nanjing 210093, China*

Hexagonal ferrites (h-RFeO$_3$) have attracted great attention for their high ferroelectric transition temperature, strong magnetoelectric couplings, and tunable Néel temperature (T_N) and electric polarization. While introducing structural distortion has been previously found to be effective to raise T_N and polarization in h-RFeO$_3$, it is generally difficult to create sizable structural distortion by common approaches including substrate-induced epitaxial strain and chemical doping. Here, we use high-pressure x-ray-diffraction measurements to show that pressure can generate large structural distortion and R-layer displacement of h-RFeO$_3$, resulting with dramatically enhancement of polarization and T_N. Density-functional theory calculations reveal that the enlarged c/a ratio results in an ∼70 K increase of T_N along with a significant enhancement of ferroelectric polarization. Our results suggest that pressure is effective to tune structural distortions and related multiferroicity of the h-RFeO$_3$ system, making h-RFeO$_3$ a promising material for spintronic applications.

Recently, multiferroicity of the hexagonal RMO$_3$ (h-RMO$_3$ with R = Y, Sc, rare-earth Lu-Dy, and M = Fe, Mn) materials has attracted great interest [1–3], especially for hexagonal RFeO$_3$ (h-RFeO$_3$) that have relatively high magnetic transition temperatures [4–9]. The coexisting spontaneous electric polarization and magnetization, along with the spin reorientation transition, render h-RFeO$_3$ compounds promising materials for multiferroic applications. In the h-RFeO$_3$ family, LuFeO$_3$ has the highest Néel temperature (T_N) of 147 K [5–9], which is still too low for room-temperature spintronic applications.

Numerous approaches have been pursued to enhance T_N [9,10]. In particular, it was proposed that increasing c/a ratio is an effective way to increase T_N [10,11]. As a matter of fact, increasing the c/a ratio in h-RMO$_3$ system results in a large structural distortion that enhances the superexchange interaction between transition-metal atoms (Fe or Mn), which is beneficial for high magnetic transition temperature [10,11]. For instance, partial substitution of Mn atoms by Fe atoms in h-LuMnO$_3$ leads to an increase of the c/a ratio from 1.885 up to 1.925 and yields an increase of T_N from 100 to 130 K [10].

Moreover, an enlarged c/a ratio and structural distortion is closely related to an enhancement of ferroelectric polarization in h-RFeO$_3$, which arises from the displacements of R-atom

(R = Y, Sc, rare-earth Lu-Dy) layers and tilting in FeO$_5$ bipyramid [11]. As reported by previous first-principles studies, applying chemical or hydrostatic pressure to hexagonal rare-earth ferrites leads to an enhanced "K_3"-mode distortion, which further results in the increase of the c/a ratio, as well as enhanced ferroelectric polarization [12]. It is highly desirable to experimentally achieve largest possible c/a ratio and thus the highest temperature at which multiferroicity can occur in h-RMO$_3$ materials.

Several methods have been utilized to tune the structure of h-RMO$_3$ systems. The substrate-induced epitaxial strain has been proven to have limited effects, due to the weak interfacial bonding between substrates and layered h-RMO$_3$ [9]. Chemical doping appears to be effective in increasing the c/a ratio of h-RMO$_3$, ranging from 1.885 in h-LuMnO$_3$ up to 1.997 in h-Lu$_{0.5}$Sc$_{0.5}$FeO$_3$ (h-LSFO) [10]. The highest T_N in the h-RMO$_3$ family has been achieved in h-LSFO, which is 172 K [10]. In the present work, we show experimentally that hydrostatic pressure can further dramatically increase the T_N and ferroelectric polarization in h-LSFO system. *In situ* high-pressure powder x-ray-diffraction (XRD) measurements unveil that (i) the hexagonal crystal structure of h-LSFO is stable up to 35.1 GPa and (ii) The hydrostatic pressure can not only increase the c/a ratio, but also increases the displacement in R-layer atoms and the tilting angle of the FeO$_5$ trigonal bipyramid, which is the main reason for the dramatically enhanced polarization and T_N. Density-functional theory (DFT) calculations show that such distortions yield a large increase in T_N and ferroelectric polarization [13]. Our study of the pressure effects on h-LSFO thus provides a powerful solution

---

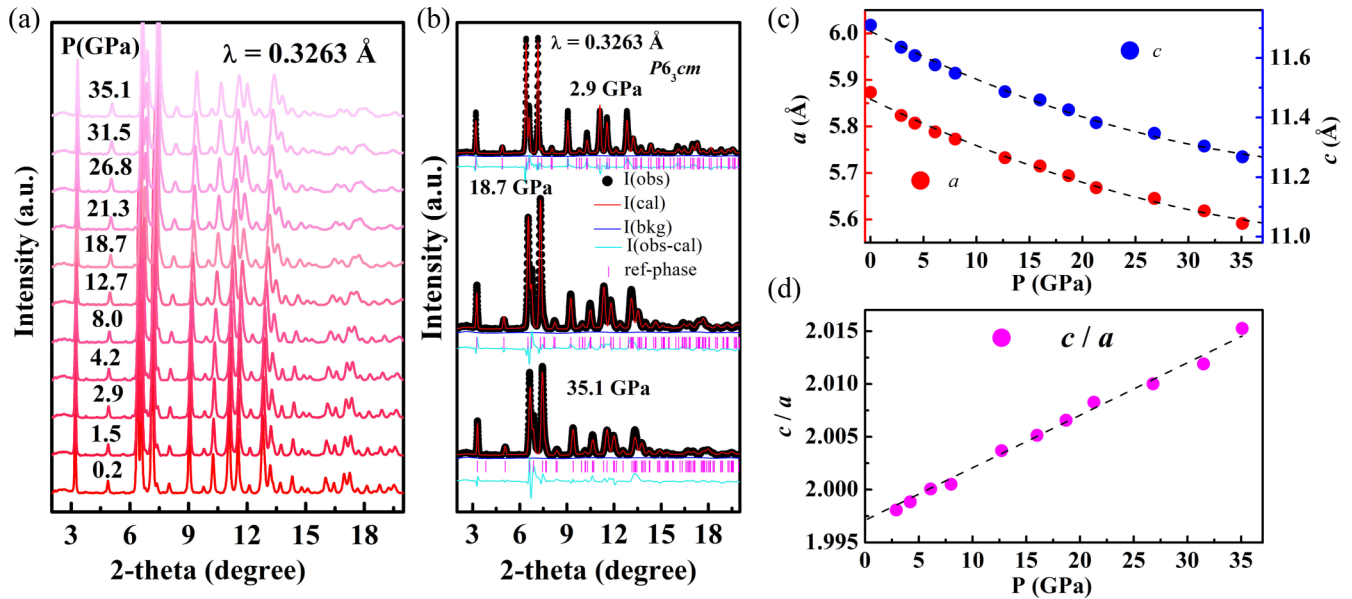*yangwg@hpstar.ac.cn
†wangwb@fudan.edu.cn
‡shenj5494@fudan.edu.cn

FIG. 1. Structural information of pressurized hexagonal $Lu_{0.5}Sc_{0.5}FeO_3$, revealed from high pressure XRD. (a) X-ray diffraction patterns collected during the compressing process, with the incident x-ray wavelength of 0.3263 Å. (b) GSAS refinement of XRD patterns at pressures 2.9, 18.7, and 35.1 GPa. (c) Lattice constant a (red) and c (blue) evolutions under pressure, with the measured data in dots, and the dashed black lines are the fitted curves. The measured lattice constants ($a = 5.8735$ Å, $c = 11.7098$ Å) at ambient conditions are also shown here. (d) c/a ratio vs pressure.

for tuning structural and physical properties of h-RMO_3 materials.

I. METHODS

The hexagonal $Lu_{0.5}Sc_{0.5}FeO_3$ (h-LSFO) single crystal was grown using the floating-zone technique. First, polycrystalline samples were prepared by a standard solid-state reaction technique. Lu_2O_3 was heated at 800 °C for 10 h before use. Stoichiometric ratios of Lu_2O_3, Sc_2O_3, and Fe_2O_3 were mixed and thoroughly ground in a mortar. The mixture was pelletized and then sintered at 1350 °C for 2 d. The resulting powder was packed into latex tubes and pressed into rods of ~5 mm in diameter and ~12 cm in length under ~300-MPa hydrostatic pressure. The obtained rods were sintered at 1380 °C for 10 h in a vertical furnace. A single crystal of $Lu_{0.5}Sc_{0.5}FeO_3$ was grown in flowing O_2 atmosphere at a pressure of 40 bar using a vertical optical image furnace (model HKZ, SciDre, GmbH, Dresden) equipped with a 3-kW Xenon arc lamp. During growth, the gas flow rate was 0.1 L/min and the upper and lower rods were counter-rotated at 23 and 29 rpm, respectively, to maintain a homogeneous melt. The crystal was grown at a speed of 1 mm/h.

Powder lab-based x-ray diffraction measurements were performed on the well-crystallized compound on a Bruker D8 Discover diffractometer ($\lambda = 1.5405$ Å) at ambient conditions. Rietveld refinement was conducted on the XRD pattern collected at ambient conditions by using the FULLPROF program [14], which indicates no impurity phases within the accuracy of powder x-ray-diffraction measurements. Zero-field-cooled and field-cooled magnetic susceptibilities of h-LSFO powder sample as a function of temperature were measured by a Physical Property Measurement System

(PPMS, Quantum Design, Inc.) in a magnetic field $H = 1000$ Oe. Ferroelectric polarization measurement on the single-crystal h-LSFO was performed at room temperature by the TF Analyzer 2000 (aix ACCT Co., Aachen, Germany) using sinusoidal wave current excitations [15].

High-pressure synchrotron powder XRD measurements were conducted at room temperature at sector 16BM-D, the Advanced Photon Source (APS), Argonne National Lab (ANL) by using the monochromatic incident x ray with the wavelength of 0.3263 Å. The powder sample was first grinded into micrometer size, and then loaded into the sample chamber shaped by rhenium gasket in the Mao-Bell diamond-anvil cell [16]. Silicone oil was used as the pressure-transmission medium for providing better hydrostatic pressure condition [17], and ruby fluorescence was used to determine the hydrostatic pressure in the sample chamber [18]. The high-pressure XRD data were collected with compression range from 0.2 up to 35.1 GPa, and decompression from 35.1 down to 0.1 GPa. The diffraction image was collected by a two-dimensional x-ray detector (MAR345) at each pressure point. Each diffraction pattern was converted into one-dimensional raw data by using the DIOPTAS software [19]. Rietveld refinement [20] analysis was performed on each pattern to get the structure information by using the GSAS software [21]. The lattice parameters were collected from GSAS refinement.

DFT calculations were performed using the Vienna *Ab initio* Simulation Package (VASP) [22]. The generalized gradient approximation and the Perdew-Burke-Ernzerhof functions for solids [23] were employed. A 500-eV plane-wave cutoff energy was used for all calculations along with the projector-augmented wave method [24], with the Lu ($5p$, $5d$, and $6s$), Sc ($3p$, $3d$, and $4s$), Fe ($3d$ and $4s$), and O ($2s$ and $2p$) electrons being treated as valence electrons. A
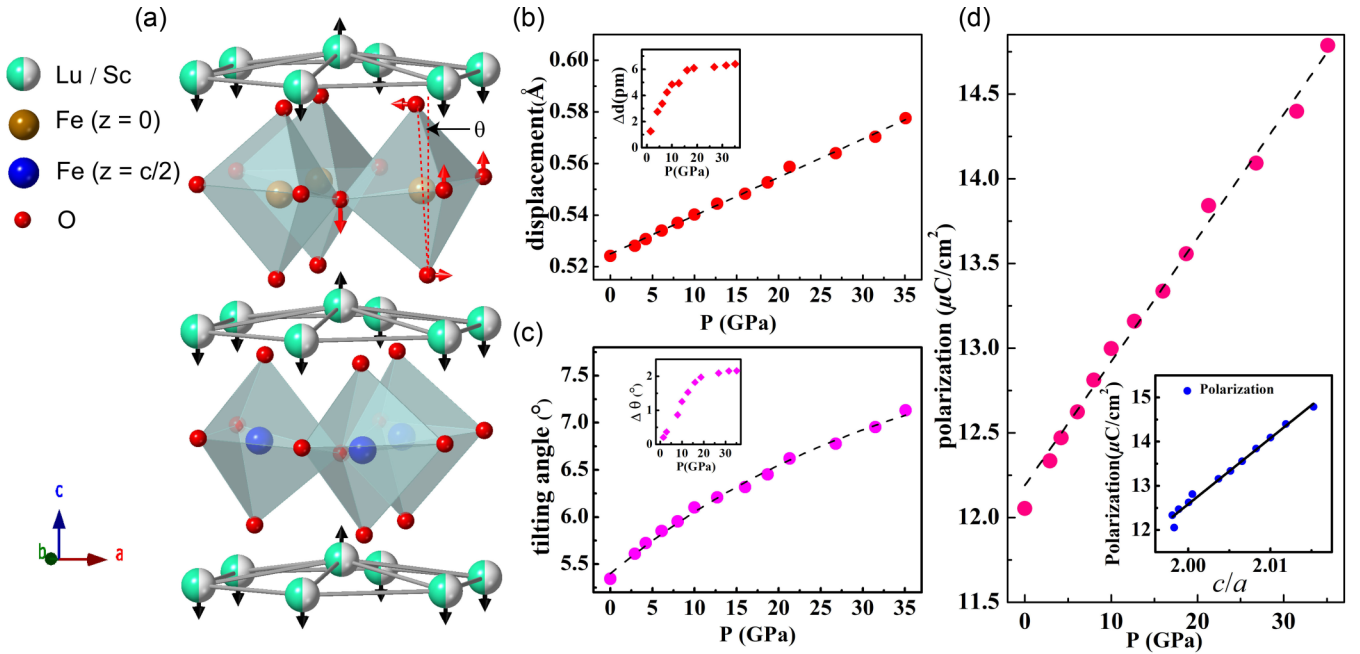
FIG. 2. DFT calculation results of some properties in pressurized h-LSFO. (a) 3D view of the crystal structure for the $P6_3cm$ hexagonal space group. The red arrows are related to the tilting of FeO_5 bipyramids associated with the K_3 mode, while the black arrows indicate the displacement of the Lu/Sc atoms within this K_3 mode. The tilting angle of FeO_5 bipyramids is denoted as θ. (b) High-pressure evolution of the displacement of Lu/Sc atoms in the Lu(Sc)-O layers and (c) tilting angle in the FeO_5 bipyramids, with the lattice parameters obtained from XRD results, while the atomic positions are optimized until all Hellman-Feynman forces are smaller than 0.01 eV/Å on each ion. Inset of (b), (c), experiment results of displacement (b) and tilting angle (c) extracted from GSAS refinement. The values along the x axis represent the pressure, labeled as P (GPa). The values along the y axis in the inset represent the experimental value of the relative [value(high pressure)-value(ambient)] displacement [(b), marked as Δd] and tilting angle [(c), marked as $\Delta\theta$]. The DFT results and the GSAS refinement results both show consistent trends of pressure-induced enhancement of displacement and tilting angle. (d) Predicted electrical polarization vs pressure (inset, polarization vs. c/a ratio).

typical effective Hubbard $U = 4$ eV was also used to treat the localized $3d$ electrons of Fe ions [25]. Moreover, a $5\times5\times3$ k-point mesh was employed for the 30-atom h-LSFO cells. The experimental lattice parameters extracted from high-pressure XRD measurement at each pressure point are adopted, while the atomic positions are optimized until all Hellman-Feynman forces are smaller than 0.01 eV/Å on each ion. Particularly, we worked on a specific (Lu, Sc) configuration that has the displacement patterns of (Lu^{up}, Lu^{down}, Sc^{down}) in one layer and (Lu^{up}, Sc^{down}, Sc^{down}) in the other layer. Such configuration has been proven to have the lowest energy among five considered possibilities in a previous work [25]. Polarizations are calculated using the Berry phase method [26].

II. RESULTS

The ambient XRD measurements show that LSFO crystallizes in the $P6_3cm$ space group (see Sec. S1 and Fig. S1 in Supplemental Material [27]) as reported before [25,28,29]. Figure 1(a) shows the diffraction patterns of h-LSFO under pressure, evidencing that the crystal structure is robust up to 35.1 GPa (see Sec. S2 in Supplemental Material [27] for detailed discussion of phase stability of o phase and h phase of RFeO₃). Upon increasing pressure, all the Bragg diffraction peaks move towards higher angles, indicating the shrinkage of lattice constants under pressure [Fig. 1(a)]. Rietveld refinement reveals that each XRD pattern within the pressure range

of 35.1 GPa can be well indexed by the original hexagonal structure $P6_3cm$, as shown in Fig. 1(b), which further demonstrates that the YMnO₃-type hexagonal structure is preserved under pressure up to 35.1 GPa.

Rietveld refinement analysis further reveals that h-LSFO is nonuniformly compressed along the a- and c-axes directions. As shown in Fig. 1(c), the lattice constant a decreases by 4.8% from 5.8735 to 5.5915 Å while the lattice constant c decreases by 3.8% from 11.7098 to 11.2683 Å, resulting in an increase of the c/a ratio to 2.015 [Fig. 1(d)]. Note that this is among the highest reported c/a ratios among the hexagonal rare-earth ferrites [9,10]. The large pressure-induced c/a ratio may be attributed to several factors: (1) The Fe $3d$-O $2p$ hybridization prefers to be along the c axis, and therefore the out-of-plane lattice constant is much more stable against pressure [30]. (2) Structural distortion of FeO_5 bipyramids may also play a significant role, as the tilting angle [θ angle demonstrated in Fig. 2(a)] increases under pressure, which is discussed in detail in Sec. S3 of Supplemental Material [27].

Previous studies demonstrated that hexagonal $Lu_{0.5}Sc_{0.5}FeO_3$ exhibits an electric polarization that is induced by geometrical displacements [25,29], which originates from the buckling of Lu/Sc atoms (one up/two down) and the tilting of FeO_5 bipyramids associated with the so-called K_3 mode. Such K_3 mode is a zone-boundary mode located at $\frac{2\pi}{a}(\frac{1}{3}, \frac{1}{3}, 0)$, where the atomic displacement of FeO_5 include the two apical oxygen atoms with opposite
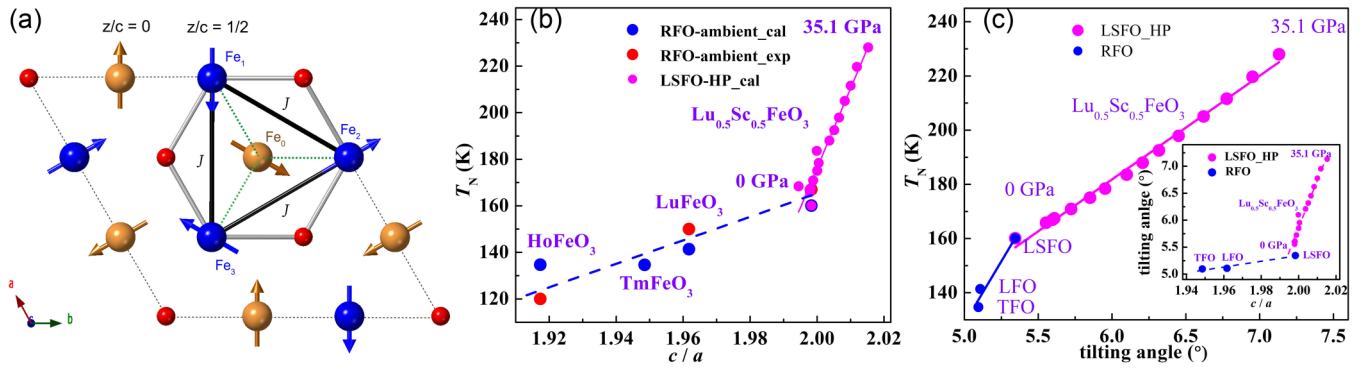
FIG. 3. Density-functional theory calculation results of the magnetic transition temperature (T_N) in h-RFeO$_3$ under chemical doping or hydrostatic pressure. (a) The nearest-neighbor (NN) superexchange interactions between in-plane Fe atoms (J), the spin structure used for calculation is consistent with Refs. [10,34]. (b) T_N vs the c/a ratio. Calculated T_N are shown via blue dots for hexagonal HoFeO$_3$ (HFO), TmFeO$_3$ (TFO), LuFeO$_3$ (LFO), and Lu$_{0.5}$Sc$_{0.5}$FeO$_3$ (LSFO) using the experimental lattice parameters for HFO [4], TFO [35], LFO [36] as inputs, while experimental results of T_N are shown via red dots for HFO [4], LFO [5–8], and LSFO (our experiment result). The calculated T_N of hexagonal Lu$_{0.5}$Sc$_{0.5}$FeO$_3$ under pressure is also displayed via magenta dots. (c) The calculated T_N vs tilting angle for h-RFeO$_3$ (blue dots) and h-Lu$_{0.5}$Sc$_{0.5}$FeO$_3$ (magenta dots), with the tilting angle vs c/a ratio being shown in the inset.

directions in the *ab* plane, and the three equatorial oxygen atoms with two up/one down along the *c* direction [11,31], which is indicated by the red arrows in Fig. 2(a). According to previous studies of RFeO$_3$ and RMnO$_3$ [12,32], It softens under pressure. Here, the GSAS (General Structure Analysis System software) refinement on the XRD patterns further shows that the Lu/Sc layers prefer to buckle under pressure, leading to a pressure-induced displacement enhancement [see inset of Fig. 2(b)]. Moreover, the GSAS refinement also suggests that the θ tilting angle [Fig. 2(a)] of nearest-neighbor interlayer FeO layers increases under pressure [see inset of Fig. 2(c)]. Therefore, the XRD data clearly indicate a pressure-induced enhancement of electric polarization in h-LSFO, as a result of this increase of the tilting angle and displacement.

DFT calculations are performed here to simulate the hydrostatic pressure effects on structural properties and electric polarization of h-LSFO. Figure 2(a) schematizes the relative displacements of Lu/Sc layers and the tilting of FeO$_5$ bipyramids, which constitute the so-called K_3 mode. As pressure is increased up to 35.1 GPa, the displacement of Lu/Sc layers increases by 11% [Fig. 2(b)], and the tilting angle of FeO$_5$ bipyramids is enhanced by 34% [Fig. 2(c)] in h-LSFO, as found from our DFT calculations. These results agree well with the GSAS refinement results of the XRD measurements (inset of Figs. 2(b) and 2(c); see Sec. S3 of Supplemental Material for details [27]). Such enhancement indicates that the strength of K_3 mode increases with increasing pressure, which is consistent with previous calculations on RFeO$_3$ and RMnO$_3$ [12,32]. The polarization, which is coupled with the K_3 mode, is determined to increase accordingly by 23%, from 12.0 μC/cm^2 at ambient pressure up to 14.8 μC/cm^2 at 35.1 GPa [Fig. 2(d)]. Such pressure-induced polarization enhancement originates from the improper nature of the ferroelectricity in hexagonal YMnO$_3$-type ferroelectrics. Therefore, in hexagonal ferrites and other improper ferroelectrics, the pressure can not only increase the c/a ratio, but also increases the displacement in R-layer atoms and the tilting angle of the

FeO$_5$ trigonal bipyramid, which is the main reason for the dramatically enhanced polarization.

Besides the electric polarization, the evolution of T_N of h-LSFO under pressure is also calculated by DFT calculations and mean-field approximation. We adopt here the magnetic Hamiltonian H $= \sum_{i,j} J\mathbf{S}_i \cdot \mathbf{S}_j$, where the summation runs over all nearest-neighbor Fe-Fe pairs. The interlayer couplings are neglected, since previous studies show that they are much weaker than intralayer couplings [25]. The coupling coefficient, J, can be extracted from the total energies of ferromagnetic and antiferromagnetic configurations. T_N can then be estimated using the equation $T_N = \frac{qJS^2}{3k_B}$, where k_B is the Boltzmann constant, $S = 5/2$ is the spin quantum number of Fe^{3+}, and $q = 6$ is the number of the nearest neighbors [33]. Note that J parameters under all pressures are rescaled by the same constant, which ensures the predicted T_N of the hexagonal LuFeO$_3$ to be consistent with the experimental value [5–8]. In addition, the spin structure used in the DFT calculation is shown in Fig. 3(a) and is consistent with the previous reported experiment results [10,34]. As shown in Fig. 3(b), the predicted T_N of the h-LSFO is 160 K at ambient pressure, which is quite close to our measured 167 K, testifying the accuracy of our calculations (once adopting the aforementioned rescaling). The calculated T_N increases monotonically with increasing pressure and reaches 228 K at 35.1 GPa, which is nearly 70 K higher than T_N at ambient condition. Moreover, Fig. 3(b) also shows that pressure has a much larger effect on T_N than chemical doping since the pressure-induced slope of T_N with increasing c/a ratio [the magenta dots and lines represent the calculated T_N of pressurized h-LSFO in Fig. 3(b)] is over 6 times larger than that induced by chemical doping [see Fig. 3(b), where the blue dots represent the calculated T_N of h-RFeO$_3$ but for which the lattice parameters are extracted from measurements [4,35,36] while the red dots display experimental results [4–8]). The dramatic enhancement of T_N can be understood from the analysis of structural distortion and tilting angle of the FeO$_5$ bipyramids. As pressure increases to 35.1 GPa, the

calculated tilting angle increases from 5.3° to 7.1° for *h*-LSFO [Fig. 2(c)], which is over 6 times larger than the increase of tilting angle induced by chemical doping [from 5.1° for TmFeO$_3$ to 5.3° for *h*-LSFO at ambient pressure, as shown in the inset of Fig. 3(c)]. As a summary of Fig. 3, it can be intuitively figured out that instead of increasing the c/a ratio, the remarkably enhanced tilting angle under pressure does matter for the dramatically T_N enhancement among the hexagonal ferrites.

We now turn to discuss the correlation between the enhanced T_N of *h*-LSFO and the structural distortion revealed by both DFT calculations and XRD measurements. As pressure increases, the distances between Fe atoms and the bond length between Fe and O atoms both decrease (see Fig. S2 [27]), leading to a stronger exchange interaction, and thus giving rise to an enhanced T_N. Besides, as pressure increases, the K_3 distortion is also enhanced, contributing to an enhancement of magnetic properties in *h*-LSFO [Fig. 3(c)], which is in line with the theory analysis proposed by Das *et al.* in hexagonal RMO$_3$ systems [11]. In addition, Sinha *et al.* also reported that T_N can be increased by enhancing structural distortion in hexagonal ScFeO$_3$ films grown on Al$_2$O$_3$ (001) substrate [37]. Moreover, the structural distortion can be much more dramatically enhanced at the case of applying hydrostatic pressure rather than the chemical doping [Fig. 3(c)] or strains arising from substrates, leading to a much more remarkable enhancement of T_N. In fact, the effectiveness of pressure to increase T_N reflects the fact that pressure has a more pronounced effect on structural distortion than previous methods (strain and chemical doping). As the crystal structure will go back to the ambient phase (see Fig. S3 [27]), and thus the T_N is also expected to go back to its value in the ambient phase. Therefore, further investigation of searching a quenchable high-pressure hexagonal phase with enhanced structural distortion and reduced Fe-Fe distance is also deserved to be done among the hexagonal ferrites and systems alike.

In conclusion, we report that, and explain why, pressure can be an effective method to enhance multiferroicity of hexagonal ferrites. In particular, pressure can lead to a large increase of T_N as well as an enhancement of the polarization in hexagonal Lu$_{0.5}$Sc$_{0.5}$FeO$_3$. According to our calculation, similar behaviors are also expected in other hexagonal systems such as RFeO$_3$ (R = Y, Sc, rare-earth Lu-Dy), and this behavior should also be valid for other hexagonal ferrites and other improper ferroelectrics.

[1] Y. Tokunaga, Y. Taguchi, T. Arima, and Y. Tokura, Nat. Phys. **8**, 838 (2012).

[2] S. Artyukhin, K. T. Delaney, N. A. Spaldin, and M. Mostovoy, Nat. Mater. **13**, 42 (2014).

[3] M. Ye and D. Vanderbilt, Phys. Rev. B **92**, 035107 (2015).

[4] A. R. Akbashev, A. S. Semisalova, N. S. Perov, and A. R. Kaul, Appl. Phys. Lett. **99**, 122502 (2011).

[5] W. Wang, J. Zhao, W. Wang, Z. Gai, N. Balke, M. Chi, H. N. Lee, W. Tian, L. Zhu, X. Cheng, D. J. Keavney, J. Yi, T. Z. Ward, P. C. Snijders, H. M. Christen, W. Wu, J. Shen, and X. Xu, Phys. Rev. Lett. **110**, 237601 (2013).

[6] J. A. Moyer, R. Misra, J. A. Mundy, C. M. Brooks, J. T. Heron, D. A. Muller, D. G. Schlom, and P. Schiffer, APL Mater. **2**, 012106 (2014).

[7] P. Suresh, K. Vijaya Laxmi, A. K. Bera, S. M. Yusuf, B. L. Chittari, J. Jung, and P. S. Anil Kumar, Phys. Rev. B **97**, 184419 (2018).

[8] S. M. Disseler, J. A. Borchers, C. M. Brooks, J. A. Mundy, J. A. Moyer, D. A. Hillsberry, E. L. Thies, D. A. Tenne, J. Heron, M. E. Holtz, J. D. Clarkson, G. M. Stiehl, P. Schiffer, D. A. Muller, D. G. Schlom, and W. D. Ratcliff, Phys. Rev. Lett. **114**, 217602 (2015).

[9] X. Xu and W. Wang, Mod. Phys. Lett. B **28**, 1430008 (2014).

[10] S. M. Disseler, X. Luo, B. Gao, Y. S. Oh, R. Hu, Y. Wang, D. Quintana, A. Zhang, Q. Huang, J. Lau, R. Paul, J. W. Lynn, S.-W. Cheong, and W. Ratcliff, II, Phys. Rev. B **92**, 054435 (2015).

[11] Hena Das, A. L. Wysocki, Y. Geng, W. Wu, and C. J. Fennie, Nat. Commun. **5**, 2998 (2014).

[12] C. Xu, Y. Yang, S. Wang, W. Duan, B. Gu, and L. Bellaiche, Phys. Rev. B **89**, 205122 (2014).

[13] Note that the fully optimized c/a ratio from simulations follows the same trend with our experimental one that the c/a ratio increases when increasing pressure.

[14] J. R. Carvajal, Physica B: Condens. Matter **192**, 55 (1993).

[15] X. F. Chen, X. L. Dong, F. Cao, J. X. Wang, and G. S. Wang, J. Am. Ceram. Soc. **97**, 213 (2014).

[16] H. K. Mao, P. M. Bell, K. J. Dunn, R. M. Chrenko, and R. C. DeVries, Rev. Sci. Instrum. **50**, 1002 (1979).

[17] S. Klotz, J.-C. Chervin, P. Munsch, and G. L. Marchand, J. Appl. Phys. D: Appl. Phys. **42**, 075413 (2009).

[18] H. K. Mao, J. Xu, and P. M. Bell, J. Geophys. Res., Solid Earth **91**, 4673 (1986).

[19] C. Prescher and V. B. Prakapenka, High Pressure Research. **35**, 223 (2015).

[20] H. M. Rietveld, J. Appl. Crystallogr. **2**, 65 (1969).

[21] B. H. Toby and R. B. Von Dreele, J. Appl. Crystallogr. **46**, 544 (2013).

[22] G. Kresse and D. Joubert, Phys. Rev. B **59**, 1758 (1999).

[23] J. P. Perdew, A. Ruzsinszky, G. I. Csonka, O. A. Vydrov, G. E. Scuseria, L. A. Constantin, X. Zhou, and K. Burke, Phys. Rev. Lett. **100**, 136406 (2008).

[24] P. E. Blöchl, Phys. Rev. B **50**, 17953 (1994).

[25] L. Lin, H. M. Zhang, M. F. Liu, S. Shen, S. Zhou, D. Li, X. Wang, Z. B. Yan, Z. D. Zhang, J. Zhao, S. Dong, and J.-M. Liu, Phys. Rev. B **93**, 075146 (2016).

[26] R. D. King-Smith and D. Vanderbilt, Phys. Rev. B **47**, 1651(R) (1993).

[27] See Supplemental Material at http://link.aps.org/supplemental/10.1103/PhysRevB.100.214408 for the details of sample characterization at ambient pressure, detailed discussion of phase stability of o phase and h phase of RFeO$_3$, details of displacement, tilting angle, and bond length evolution results extracted from GSAS refinement, and the detailed discussion of XRD patterns collected during decompress process.

[28] A. Masuno, A. Ishimoto, C. Moriyoshi, H. Kawaji, Y. Kuroiwa, and H. Inoue, Inorg. Chem. **54**, 9432 (2015).

[29] K. Du, B. Gao, Y. Wang, X. Xu, J. Kim, R. Hu, F.-T. Huang, and S.-W. Cheong, npj Quantum Mater. **3**, 33 (2018).

[30] S. Cao, X. Zhang, T. R Paudel, K. Sinha, X. Wang, X. Jiang, W. Wang, S. Brutsche, J. Wang, P. J Ryan, J.-W. Kim, X. Cheng, E. Y Tsymbal, P. A Dowben, and X. Xu, J. Phys.: Condens. Matter **28**, 156001 (2016).

[31] H. Wang, I. V. Solovyev, W. Wang, X. Wang, P. J. Ryan, D. J. Keavney, J.-W. Kim, T. Z. Ward, L. Zhu, J. Shen, X. M. Cheng, L. He, X. Xu, and X. Wu, Phys. Rev. B **90**, 014436 (2014).

[32] H. Tan, C. Xu, M. Li, S. Wang, B.-L. Gu, and W. Duan, J. Phys.: Condens. Matter **28**, 126002 (2016).

[33] S. V. Halilov, H. Eschrig, A. Y. Perlov, and P. M. Oppeneer, Phys. Rev. B **58**, 293 (1998).

[34] J. C. Leiner, T. Kim, K. Park, J. Oh, T. G. Perring, H. C. Walker, X. Xu, Y. Wang, S.-W. Cheong, and J.-G. Park, Phys. Rev. B **98**, 134412 (2018).

[35] A. A. Bossak, I. E. Graboy, O. Y. Gorbenko, A. R. Kaul, M. S. Kartavtseva, V. L. Svetchnikov, and H. W. Zandbergen, Chem. Mater. **16**, 1751 (2004).

[36] E. Magome, C. Moriyoshi, Y. Kuroiwa, A. Masuno, and H. Inoue, Jpn. J. Appl. Phys. **49**, 09ME06 (2010).

[37] K. Sinha, H. Wang, X. Wang, L. Zhou, Y. Yin, W. Wang, X. Cheng, D. J. Keavney, H. Cao, Y. Liu, X. Wu, and X. Xu, Phys. Rev. Lett. **121**, 237203 (2018).